Materials Science & Engineering C 121 (2021) 111891

Contents lists available at ScienceDirect

Materials Science & Engineering C

journal homepage: www.elsevier.com/locate/msec

Nano-synergistic combination of Erlotinib and Quinacrine for non-small cell lung cancer (NSCLC) therapeutics – Evaluation in biologically relevant in-vitro models

Nishant S. Kulkarni [a,1], Bhuvaneshwar Vaidya [b,1,2], Vivek Gupta [a,b,*]

[a] College of Pharmacy and Health Sciences, St. John's University, Queens, NY 11439, USA
[b] School of Pharmacy, Keck Graduate Institute, Claremont, CA, USA

ARTICLE INFO

Keywords:
Synergy
Combination therapy
Erlotinib
Quinacrine
Nanoparticles
NSCLC

ABSTRACT

Non-small cell lung cancer (NSCLC), pre-dominant subtype of lung cancer, is a global disorder affecting millions worldwide. One of the early treatments for NSCLC was use of a first-generation tyrosine kinase inhibitor, Erlotinib (Erlo). However, chronic exposure to Erlo led to development of acquired drug resistance (ADR) in NSCLC, limiting the clinical use of Erlo. A potential approach to overcome development of ADR is a multi-drug therapy. It has been previously reported that Erlo and Quinacrine (QA), an anti-malarial drug, can work synergistically to inhibit tumor progression in NSCLC. However, the combination failed at clinical stages, citing lack of efficacy. In this study, an effort has been made to improve the efficacy of Erlo-QA combination via development of nanoformulations, known to enhance therapeutic efficacy of potent chemotherapies. Synergy between Erlo and QA was measured via estimating the combination indices (CI). It was seen that established combination of nanoformulations (CI: 0.25) had better synergy than plain drug solutions (CI: 0.85) in combination. Following extensive in-vitro testing, data were simulated in biologically relevant 3D tumor models. Two tumor models were developed for extensive in-vitro testing, 3D-Spheroids grown in ultra-low attachment culture plates for efficacy evaluation and a 5D-spheroid model in 5D-sphericalplate with capability of growing 750 spheroids/well for protein expression analysis. Extensive studies on these models revealed that combination of Erlo and QA nanoformulations overall had a better effect in terms of synergy enhancement as compared to plain drug combination. Further, effect of combinatorial therapy on molecular markers was evaluated on 5D-Sphericalplate leading to similar effects on synergy enhancement. Results from present study suggests that combination of nanoformulations can improve the synergy between Erlo and QA while reducing the overall therapeutic dose.

1. Introduction

Non-Small Cell Lung Cancer (NSCLC) affects millions of people worldwide and is one of the deadliest cancer types with high mortality rate and poor diagnosis [1]. NSCLC tumors have a complicated multi-faceted mechanism for survival which involves numerous signaling and proliferation pathways [2,3]. Some of these pathways are well understood and studied but many of them are yet to be explored; and this incomplete knowledge may be the reason for such poor prognosis of NSCLC. Some common survival pathways for NSCLC are the epidermal growth factor receptor (EGFR) mediated pathways, which are deemed to be the most essential survival pathways [4]. One of the first-generation drugs approved for NSCLC treatment was Erlotinib (Erlo) in the form of an oral tablet (Tarceva®), which acts via inhibition of EGFR tyrosine kinase [5]. Tarceva® was first approved in 2004 and since then has been a potent tool used to combat NSCLC [6]. Recently in 2016, the FDA limited use of Tarceva® only to patients with EGFR mutated NSCLCs [7]. This limitation in the use of Tarceva® can be attributed to the fact that prolonged Erlo treatment often leads to specific genetic mutations at certain amino acid residues leading to acquired drug resistance (ADR) [8]. Such mutations can render even the most potent molecules ineffective. Some commonly known mutations in EGFR are T790M, BRAF, KRAS, etc. [9–11], occurring at specific amino acid residues in proteins on chronic chemotherapeutic exposure.

* Corresponding author at: College of Pharmacy and Health Sciences, St. John's University, 8000 Utopia Parkway, Queens, NY 11439, USA.
E-mail address: guptav@stjohns.edu (V. Gupta).
[1] Equal contribution.
[2] Current Address: School of Pharmacy, Texas Tech University Health Science Center, Amarillo, TX – 79106, USA.

https://doi.org/10.1016/j.msec.2021.111891
Received 2 November 2020; Received in revised form 7 January 2021; Accepted 10 January 2021
Available online 15 January 2021
0928-4931/

Aggressive innovations in the field of drug discovery are taking place to come up with newer and safer molecules for NSCLC therapy. One of the discovery approaches is repositioning existing FDA approved drugs for NSCLC treatment [12–14]. If potent, repositioning an already approved and safe drug saves a lot of time and finances involved in preclinical and clinical safety testing [15]. One such repositioned drug is Quinacrine (QA), a globally approved anti-malarial drug, which has been reported to be effective in treatment of multiple types of cancers [16–18]. QA has been reported to be an effective modulator of autophagic and apoptotic pathways along with potency via DNA intercalation, and tumor suppressor activation via p53 gene among many other reported pathways [19–21]. This shows the versatility of QA against cancer and its poly-pharmacological nature as a molecule. Apart from being an effective standalone therapy, QA has also been reported to help overcome Erlo induced ADR by sensitizing cells to Erlo therapy and synergizing along with Erlo [22,23]. Embracing a synergistic approach for chemotherapy can help tackle any form of cancer via simultaneous efficacy against multiple pathways [24]. A complex multifaceted framework of pathways for progression of NSCLC necessitates the need for a synergistic approach to curb its aggressive metastasis.

Despite being a poly-pharmacological agent capable of synergizing with Erlo, QA has several issues such as poor bioavailability due to limited absorption, and yellow pigmentation of skin along with certain immunological responses [20]. Erlo on the other hand is also shadowed by bioavailability issues pertaining to its limited aqueous solubility [25]. These issues cite the need for development of safe and effective carriers for both the drugs which can help in exploiting their full potential against NSCLC. Development of polymeric nanocarriers has been an effective and safe technique to improve bioavailability and curb off-target toxic effects via channeling the dose toward the site of action [26]. Such carriers also exhibit an enhanced intracellular accumulation in cancer cells which can be attributed to the enhanced permeation and retention (EPR) effect theorized for nanoformulations [27]. An enhanced intracellular accumulation also curbs the dose requirements for potent molecules, further reducing toxic effects. Utility of biodegradable polymers such as poly lactic-*co*-glycolic acid (PLGA) further establishes the safety of the nanoformulations [28]. All in all, development of a polymeric nano system is beneficial for safe and efficacious delivery of a synergistic NSCLC therapy.

This extensive in-vitro testing report has been carried out on biologically relevant (bio-relevant) tumor models which mimic physiological conditions as closely as possible. Development of bio-relevant in-vitro tumor models has been on the rise since the past decade due to social concerns surrounding animal safety. Moreover, lack of robust in-vitro tumor models leads to inaccurate dose predictions for pre-clinical in-vivo studies. This in turn increases the number of animals needed for testing to accurately predict the dose. Availability of a robust and physiologically similar 3D tumor model would help in overcoming all the aforementioned issues and additively being cost effective. Such in-vitro models can also be used for predicting in-vivo dose for the therapy. Recent advancements in development of bio-relevant models have given rise to multiple robust techniques to form these tumor spheroids in a plate. Methods like hanging drop, liquid overlay, microfluidics, rotating well culture etc. have been developed [29]. Moreover, novel materials have been also utilized to closely mimic physiological structures like bones [30] and this can be combined with tumor models to mimic the entire physiological framework for disease conditions like tumors in different regions of the body.

Recently, nanoformulations for both QA and Erlo were established and reported by our group as standalone therapies for NSCLC [31,32]. QA-NPs were developed to have a surface positive charge via inclusion of polyethyleneimine (PEI); and Erlo-NPs were prepared by loading an Erlo-Cyclodextrin complex to improve solubility issues of Erlo. Both formulations reported desirable physical characteristics in terms of size and charge along with a diverse release profiles, and high degree of anticancer efficacy in comparison to plain drug therapy. In this study, these reported formulations are reproduced and combined to attain a safe and efficacious synergistic therapy for attenuating the progression of NSCLC.

2. Materials

Quinacrine dihydrochloride (QA) was procured from Sigma-Aldrich (St. Louis, MO, USA), Erlotinib hydrochloride (Erlo) was obtained from LC Labs (Woburn, MA, USA). Poly-lactic co-glycolic acid 50:50 (PLGA) was procured from Akina Inc. (West Lafayette, IN, USA) and Resomer 502H was procured from Sigma-Aldrich (St. Louis, MO, USA). Sulfobutylether-cyclodextrin (SBECD) was procured from Cydex Pharmaceuticals (Lawrence, Kansas, USA) RPMI-1640 cell growth medium along with sodium pyruvate, penicillin-streptomycin and trypsin were obtained from Corning (Corning, NY, USA), Fetal bovine serum was obtained from Atlanta Biologicals (Flowery Branch, GA, USA), 3-(4,5-dimethylthiazol-2-yl)-2,5-diphenyl tetrazolium bromide (MTT) was obtained from Fisher Scientific (Waltham, MA, USA). Crystal violet dye was obtained from Fisher Chemicals (Hampton, NH, USA), Live/Dead viability assay kit was obtained from Biotium (Fremont, CA, USA). Propidium iodide dye was obtained from Life technologies (Carlsbad, CA, USA), RNAse/DNAse was obtained from Thermo Fisher Scientific (Waltham, MA, USA). CYTO-ID® autophagy detection kit was obtained from Enzo Life Sciences (Farmingdale, NY, USA). Pre-cast 4–20% TGX 15 well Gels and Midi PVDF transfer packs were obtained from Bio-Rad Laboratories (Hercules, CA, USA). All other reagents were of analytical grade and were purchased from third-party vendors. Sources for all the antibodies are provided in respective sections.

3. Methods

3.1. Cell culture studies

In this study, A549, an immortalized NSCLC cell line procured from American Type Culture Collection (ATCC, Manassas, VA, USA), was used to perform extensive in-vitro efficacy testing. A549 was cultured using RPMI-1640 cell growth medium supplemented with 10% Fetal Bovine Serum, 1% sodium pyruvate and 1% penicillin-streptomycin. The cells were grown at 37 °C/5% CO_2 in tissue culture (TC) treated T75 cell culture flasks (Eppendorf, Hauppauge, NY, USA) until 80–85% confluency was reached. Confluent cells were trypsinized and used for in-vitro experiments. Immortalized cell lines were used until 20–25 passages to maintain experimental integrity.

3.2. Evaluation of synergistic potential of Erlotinib (Erlo) and Quinacrine (QA) in NSCLC

To evaluate the synergistic potential of Erlo and QA in NSCLC cell lines in-vitro, two sets of experiments were designed based on dosing strategy. Briefly, A549 cells were seeded in TC-treated 96-well plates (2,500 cells/well) and were allowed to attach overnight. Following day, the first strategy was to treat A549 cells with Erlo (1.87-, 3.75-, and 5-μM) and QA (0.37-, 0.75-, and 1-μM) concurrently, while the other strategy involved sensitizing the cells with QA for 6 h prior to Erlo treatment. Treatments were ended at 24 h, 48 h and 72 h. At the end of treatment, % cell viability was determined by MTT assay, as reported earlier [33]. Briefly, the media was aspirated from the wells, and cells were incubated with 100 μL of MTT solution (1 mg/mL in sterile PBS) for 2 h. Subsequently, MTT solution was aspirated and 100 μL of DMSO was added to dissolve formazan crystals in each well. The plates were then shaken for 30 min, and absorbance was read on a Spark 10 M (Tecan, Männedorf, Switzerland) plate reader at 570 nm. Combination index of Erlo and QA was calculated using CompuSyn software (ComboSyn, Inc.).

3.3. Development and optimization of drug-loaded plga nanoparticles

PEI-Stabilized QA-loaded (QA-NPs) and Erlo-loaded PLGA

nanoparticles (Erlo-NPs) were prepared using previously reported methods [31,32]. For Erlotinib loaded nanoparticles, Erlo was complexed with 4% sulfobutylether-cyclodextrin (SBECD; Erlo-CD), and was selected over plain Erlo due to enhanced therapeutic activity, as reported [31]. Briefly, both formulations contained PLGA 50:50 polymer (Resomer 502H for Erlo and Polyscitech PLGA 50:50 for QA; 20 mg/mL) dissolved in dichloromethane (3 mL) to form organic phase. Aqueous QA/Erlo-CD solution was used as internal aqueous phase. 2% Polyethyleneimine (PEI) in 2% PVA was used as an external aqueous phase for QA-loaded particles, and 2% PVA was used as an external phase for Erlo-loaded particles. For both formulations, internal aqueous phase was added dropwise in the polymer solution and sonicated for 2 min using a probe sonicator (40% amplitude; 10 s on/off cycle; QSonica Q500, Newtown, CT, USA) to form a primary emulsion. Primary emulsion was further added to external aqueous phase and sonicated for 4 min to form w/o/w multiple emulsion (10 s on/off cycle). Organic solvent was evaporated using rotary vacuum evaporator. Organic solvent-free nanoparticles were collected by refrigerated centrifugation at 21,000 $\times g$ for 15 min and washed with water thrice followed by resuspending in water to 1 mL volume.

3.4. Physical characterization of drug loaded PLGA nanoparticles

Prepared nanoparticles were characterized for their size, zeta potential (DLS Zetasizer, Malvern Inc., UK), entrapment efficiency, release profiles and morphology. For both nanoformulations, in-vitro release data and transmission electron microscopy (TEM) images were reproduced with permission from previous publications [31,32].

3.4.1. Particle size and zeta potential analysis

Particle size distribution and surface charge evaluation for prepared Erlo-NPs and QA-NPs was done using dynamic light scattering particle size analyzer (DLS Zetasizer, Malvern, UK). Polydispersity indices (PDI) were evaluated to assess the uniformity in nano-sized particles. Surface charge was evaluated by measuring the zeta potential of developed particles.

3.4.2. Evaluation of entrapment efficiency and drug loading

Entrapment efficiency was quantified by lysing the particles and analyzing the entrapped drug using reversed phase ultra-performance liquid chromatography (UPLC; Waters, Inc., Milford, MA, USA). For QA-loaded particles, 0.1% o-phosphoric acid:acetonitrile (35:65) was used as a mobile phase [32] and analyzed at 346 nm, whereas for Erlo-NPs, 0.1% o-phosphoric acid+0.1% triethylamine: acetonitrile (10:90) was used as the mobile phase and analyzed at 247 nm. Retention time for QA was 0.5 min and that for Erlo was 1.7 min respectively. The following equation was used to calculate the entrapment efficiency (EE) and % loading efficiency (%LE) of the particles:

$$EE\% = \left[\frac{Total\ drug\ taken\ initially - unentrapped\ drug}{Total\ drug\ taken\ initially}\right] \times 100$$

$$\%LE = \left[\frac{Total\ amount\ of\ drug\ entrapped}{Total\ amount\ of\ nanoparticles}\right] \times 100$$

3.4.3. In-vitro drug release studies for Erlo-NPs and QA-NPs

In-vitro drug release studies for both Erlo-NPs and QA-NPs were carried out by resuspending specific amounts of lyophilized nanoparticles in 1.5 mL of phosphate buffer saline (pH 7.4) in microcentrifuge tubes, which were incubated at 37 °C at 50 rpm for various time intervals. At each time point, desired tubes were centrifuged, and the supernatant was analyzed on UPLC for drug release.

3.4.4. Morphological evaluation of Erlo-NPs and QA-NPs

For transmission electron microscopy (TEM), 300-mesh Formvar® carbon-coated copper grids (Electron Microscopy Sciences, Hatfield, PA, USA) were made hydrophilic using glow discharge plasma treatment for 30 s. Approximately 5 μL of dilute nanoparticle suspension (for both Erlo-NPs and QA-NPs) was placed on the treated grids and allowed to dry at room temperature. TEM micrographs were obtained using JEOL 1230 TEM (JEOL USA, Peabody, MA, USA) operated at 120 kV.

3.5. Evaluation of intracellular co-localization of nanoparticles

Cellular uptake studies were performed to evaluate the internalization efficiency of combination of two nanoparticle systems, as reported earlier [34]. Briefly, A549 cells were plated in tissue culture (TC) treated cell imaging 8-chambered cover-glass (Eppendorf, Hauppauge, NY, USA) at a seeding density of 10,000 cells/chamber followed by overnight incubation. Following day, cells were incubated with QA-loaded NPs, and Texas red NPs (simulating Erlo-NPs, prepared in a similar way as mentioned in the previous section); plain QA and Texas red as controls for a period of 3 h. After 3 h, cells were washed with ice-cold sterile PBS twice and fixed with 4% PFA for 10 min. Fixed cells were washed again with ice-cold PBS twice and chambers were carefully removed. Sufficient Vectashield hardset mount with DAPI nuclear stain (H1500, Vector laboratories, Burlingame, CA, USA) was placed on a glass slide dropwise followed by the cell containing cover glass placement. After hardening of mounting medium, the cells were imaged using an EVOS-FL microscope 20× objective (Thermo Scientific, Waltham, MA, USA).

3.6. Evaluation of cytotoxic potential of Erlotinib and Quinacrine loaded nanoparticles' combination therapy

After establishing the synergy between Erlo and QA, it was essential to establish an enhanced efficacy profile of the synergy using delivery systems. QA-NPs (0.37-, 0.75- and 1-μM) and Erlo-NPs (1.87-, 3.75- and 5-μM) were used in combination on A549 cells to test cellular viability. Briefly, cells were grown in 10% FBS supplemented RPMI-1640 media as described in the *Materials* section, seeded in TC treated 96-well plates (Eppendorf, Hauppauge, NY, USA) (2,500 cells/well) and were incubated overnight for adherence at 37 °C/5% CO_2. Following day, adhered cells were treated with varying concentrations of combination therapy along with mono-therapy controls. After all time points, % cell viability was determined by MTT assay as described above.

3.7. Effect of Erlo-NP and QA-NP combination on cellular colony formation: clonogenic assay

Clonogenic assay is an in-vitro cell survival assay which is based on a small group of cells' capabilities to grow into individual colonies. Following a protocol reported earlier [35], A549 cells were seeded into 6-well culture plates at a seeding density of 500 cells/well followed by overnight incubation for cellular adhesion. Next day, cells were treated with QA (1 μM), Erlo (5 μM) QA + Erlo (1 μM + 5 μM) solution and QA-NP + Erlo-NPs (1 μM + 5 μM) for 48 h. After 48 h, all treatments were removed, and fresh media replacements were done on alternative days for a 7-day period. On the 7th day, media was removed from all the wells and colonies were stained with crystal violet following published protocols [36]. After staining, cells were washed with distilled water and images were captured using a digital camera. Cell colonies were counted by colony counter software Open CFU [37].

3.8. Effect of combination therapy on viability of a 3D-spheroid cell based model

3D cell-based tumor spheroids were developed as previously reported for evaluating the effect of combination therapy on NSCLC prognosis [38]. Briefly, A549 cells were trypsinized on reaching 80% confluency and plated in 96-well ultra-low attachment U-shaped plates (2,000 cells/well) (Corning Inc., Corning, NY, USA). Cells were allowed

to form spheroids for three days followed by treatment with QA (1 μM), Erlo (5 μM), QA + Erlo (1 μM + 5 μM) solution and QA-NP + Erlo-NP (1 μM + 5 μM). Spheroids were dosed in two ways, single dose and multiple dose [39]. Media replenishment and dosing was done every 72 h. Images were captured every 72 h using an inverted color microscope (10× objective) (Laxco, Mill Creek, WA, USA) for 15 days.

At the end of treatment period, live/dead assay was performed for spheroids using a viability/cytotoxicity assay kit (Biotium, Fremont, CA, USA) as per manufacturer's protocol. Live cells were stained green by calcein AM and dead cells were stained red by ethidium homodimer III (EthD-III), and spheroids were imaged using an Evos FL fluorescence microscope (4× objective) (Thermo Fisher Scientific, Waltham, MA, USA) using GFP (green fluorescence protein) and RFP (red fluorescence protein) filters respectively.

3.9. Cell cycle analysis by flow cytometry

Cell cycle analysis was done using propidium iodide staining. Briefly, A549 cells were seeded in TC-treated 100 mm dishes (500,000 cells/dish, $n = 3$) and incubated overnight for attachment. Following day, cells were treated with QA (1 μM), Erlo (5 μM), QA + Erlo (1 μM + 5 μM) solution or QA-NP + Erlo-NP (1 μM + 5 μM). After 24 h, treatments were removed, and cells were washed thoroughly with 1× PBS followed by trypsinization for cell harvesting. Cell pellets were collected and fixed with 70% ice-cold ethanol for 2 h. Following fixing, cells were washed with 1× PBS and incubated with RNA-se (10 mg/mL) for 45 min at 37 °C followed by overnight incubation with Propidium Iodide (1 mg/mL) in dark. Cells were then analyzed (10,000 counts/sample) using BD Accuri™ C6 (BD Biosciences, San Jose, CA, USA). Data were analyzed using FlowJo software.

3.10. Effect of combination therapy on autophagy inhibition in NSCLC

Effect of QA + Erlo combination on autophagy inhibition was tested in-vitro using CYTO-ID® Autophagy Detection Kit. Briefly, A549 cells were seeded in 96-well plates (2.5×10^5 cells/mL) and were supplemented with serum-free media to induce starvation linked autophagy process for 24 h. After 24 h, starved cells were treated with QA (1 μM), Erlo (5 μM), QA + Erlo (1 μM + 5 μM) solution or QA-NP + Erlo-NP (1 μM + 5 μM) for 18 h, as optimized previously [36]. Treatments were then replaced with 1× assay buffer (100 μL) followed by addition of dual color detection reagent and incubated for 30 min in dark at 37 °C (100 μL of CYTO-ID® Green Detection Reagent + Hoechst 33342 nuclear stain growth medium without phenol red indicator supplemented with 5% FBS). CYTO-ID® Green Detection Reagent was read with a FITC filter (480 nm/530 nm ex/em), and Hoechst 33342 Nuclear Stain was read with a DAPI filter set (340 nm/480 nm ex/em) using a Tecan Spark 10 M plate reader.

3.11. Effect of combination therapy on cellular apoptosis via evaluation of caspase-3 levels

Levels of caspase-3, a molecular marker induced in apoptotic events, was measured using an EnzChek™ Caspase-3 Assay Kit (Molecular Probes, Eugene, OR, USA) as per the manufacturer's specifications. Briefly, A549 cells were seeded at a density of 1×10^6 cells/TC dish of a 100-mm diameter dish (Thermo Scientific, Rochester, NY, USA) and treated with QA (1 μM), Erlo (5 μM), QA + Erlo (1 μM + 5 μM) solution or QA-NP + Erlo-NP (1 μM + 5 μM) for 6 h followed by harvesting and washing of cell pellets. Cell lysis was carried out using 1× cell lysis buffer and placing cell samples in ice for 30 min, followed by centrifugation. Supernatants obtained were transferred to a 96-well plate to which 50 μL of 2× substrate working solution (10 mM *Z*-DEVD-AMC substrate +2× reaction buffer) was added and incubated for 20 min. Fluorescence was then measured at excitation/emission 360/440 nm.

3.12. Effect of Erlotinib- and Quinacrine-loaded nanoparticles on NSCLC molecular markers

A549 cells were plated (1×10^6 cells/petri dish) and were treated with QA (1 μM), Erlo (5 μM), QA + Erlo (1 μM + 5 μM) solution, or QA-NP + Erlo-NP (1 μM + 5 μM) at 37 °C/5% CO_2 for 72 h. After treatment, the cells were collected and lysed with 1% Triton® X-100 and 1% Halt™ Protease and Phosphatase Inhibitor Cocktail in PBS, and bath sonicated for 1 h at 4 °C. Samples were centrifuged for 15 min at 4 °C at 15,000 rpm and lysates were collected. Cell lysate protein was quantified by the DC™ Protein Assay Kit (Bio-Rad, Hercules, CA, USA). The samples were mixed with 2× Laemmli buffer and 2-mercaptoethanol, and denatured at 100 °C for 10 min. For Western blot analysis, 25 μg protein was loaded and separated on 4%–20% Mini-PROTEAN® TGX™ Precast Protein Gels at a voltage of 135 mV for 60 min followed by transfer to Midi PVDF membranes using a Bio-Rad Trans-Blot® Turbo™ system. Membranes were blocked with 5% bovine serum albumin in PBS and probed with corresponding antibodies overnight at 4 °C. The following antibodies were used: β-actin (CST, #8457S) (1:1000), LC3-B (CST, #3868S) (1:500) and NF-κB (CST, #8242S) (1:500). Membranes were then incubated with corresponding secondary HRP-conjugated anti-rabbit antibody (Life Technologies, Carlsbad, CA, USA) (#32260, 1:10000) for 1 h at room temperature and subjected to chemiluminescence. Protein signals were detected on the membranes and were quantified using the chemiluminescent imaging by the Omega Lum™ G Imaging System (The Gel Company, San Francisco, CA, USA). The band intensities were analyzed using ImageJ open source software.

3.13. Effect of combination therapy on molecular markers from a 5D-spheroid cell based model

To evaluate the effect of combination therapy on molecular markers in a 5D-Spheroid tumor model, a 5D-Sphericalplate (Kuglemeiers, Erlenbach, Switzerland) was used to grow tumor spheroids of A549 cells. This specially designed plate can hold up to 750 spheroids/well (9,000 spheroids/plate). Briefly, 2,000 cells/well were seeded and the spheroids were allowed to settle and form for a week. Followed by this, spheroids were treated with QA (1 μM), Erlo (5 μM), QA + Erlo (1 μM + 5 μM) solution or QA-NP + Erlo-NP (1 μM + 5 μM) as a single dose and incubated for 12 days with media replenishments every 72 h. After 12 days, the spheroids were collected and a similar procedure to western blotting was followed, as mentioned in the earlier section. LC3-B and NF-κB was studied for their expression levels.

3.14. Statistical analysis

All data presented here are mean ± SD or SEM ($n = 3$–6). Cytotoxicity studies represent average of 3 independent trials ($n = 6$ for each trial). Unpaired student's *t*-test was used to compare two groups whereas to compare more than two groups one-way ANOVA followed by Tukey's post hoc multiple comparison test was used. $p < 0.05$ was considered statistically significant and are reported throughout the manuscript.

4. Results

4.1. Quinacrine and Erlotinib exhibit higher synergy when QA sensitizes cells prior to Erlo administration

Three concentrations of QA (0.37-, 0.75-, and 1-μM) were hand-picked based on the cytotoxicity potential reported in our previous study [32] and combined with three concentrations of Erlo (1.87-, 3.75-, and 5-μM). Dermawan et al. reported that for optimum synergy, QA to Erlo ratio should be 1:5 [22], and this was tested as seen in Fig. 1A. The effect of incubating Erlo and QA together i.e. "co-incubation" versus sensitizing the cells with QA for 6 h followed by Erlo treatment i.e. "pre-incubation" was studied (Fig. 1A). This knowledge would help better

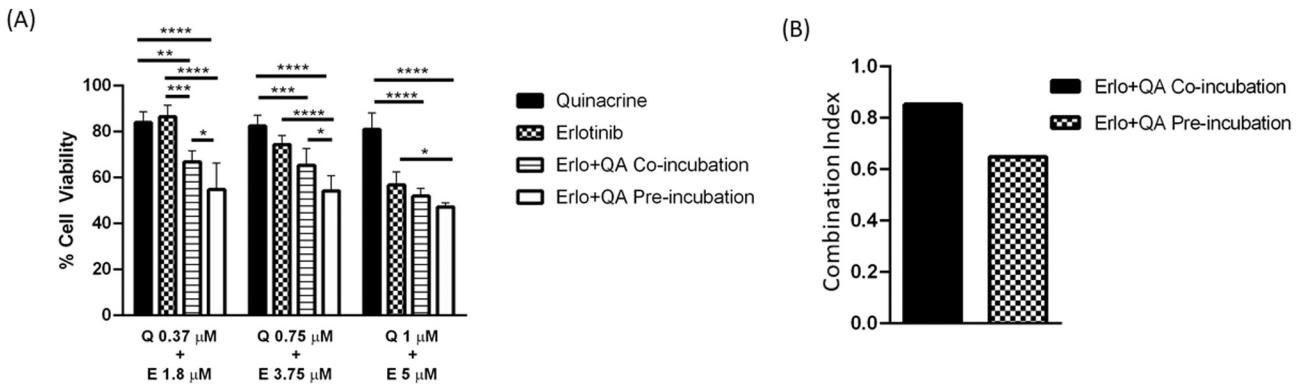

Fig. 1. (A) Represents cytotoxicity data for plain drug solutions, as compared to combination of QA and Erlo, tested on A549 cells. Two types of administration strategies were tested, a co-incubation strategy and QA pre-incubation strategy to sensitize cells prior to Erlo treatment. It can be seen QA pre-incubation strategy has higher efficacy in killing A549 cells as compared to co-incubation strategy. Both strategies were more efficacious than mono therapy. Cytotoxicity was measured using MTT assay. (B) Plot represents combination indices for co-incubation and pre-incubation strategy. Lower CI values indicate higher synergy. Data are presented as % cell viability and represent mean ± SD (average of 3 individual experiment with $n = 6$) (*$p < 0.05$, **$p < 0.01$, *** $p < 0.001$, **** $p < 0.0001$).

understand the correct dosing strategy for QA + Erlo combination to obtain maximum therapeutic potential. It can be clearly seen that for all tested combination concentrations, sensitization of A549 cells with QA 6 h prior to Erlo treatment yielded better therapeutic effects than concurrent QA and Erlo therapy. A significant difference between co-incubation and pre-incubation strategies was observed at all concentrations as follows; QA 0.37- and Erlo 1.8 μM: 66.8 ± 4.7% viability for co-incubation versus 54.7 ± 11.5% cell viability for pre-incubation ($p < 0.05$); QA 0.78- and Erlo 3.75 μM: 65.3 ± 7.2% viability for co-incubation versus 54.1 ± 6.6% cell viability for pre-incubation ($p < 0.05$); QA 1- and Erlo 5 μM: 51.9 ± 3.3% viability for co-incubation versus 47.1 ± 1.8% cell viability for pre-incubation (*ns*) (Fig. 1A). The combination indices were separately calculated for plain drug solutions for both co- and pre-incubation strategies. Co-incubation combination index (CI) for QA + Erlo was found to be 0.8525 which was in agreement with the study conducted by Dermawan et al.. Pre-incubation strategy resulted in a significantly stronger synergy, as confirmed from cytotoxicity data with a CI of 0.6485 (Fig. 1B). It can be clearly seen that combination therapy had significantly better therapeutic efficacy than plain drugs at the same concentrations. Along with this, it was established that pre-incubation sensitization with QA prior to Erlo treatment was an ideal strategy for this combinatorial. Elaborated data for cytotoxicity of all concentration combination is represented in Fig. S1. This proof-of-concept study laid ground for optimizing nanoparticle formulations to enhance the QA + Erlo synergy.

4.2. Development and optimization of nano-engineered delivery systems for Quinacrine (QA) and Erlotinib (Erlo)

Erlo-NPs and PEI-Stabilized QA-NPs (QA-NPs) were separately formulated and reproduced as reported earlier [31,32]. The main aim of this study was to study the combinatorial effect of developed nanoparticles, and hence no alteration was made to already established formulations.

4.2.1. Particle size and surface charge analysis of Erlo-NPs and QA-NPs

Prepared Erlo-NPs and QA-NPs were re-characterized for their particle size and surface charge to ensure appropriate physical characteristics to achieve maximum therapeutic potential, when administered as a combination. Erlo-NPs had a mean particle size of 198 ± 6 nm with a surface charge of −26 ± 3 mV. On the other hand, QA-NPs had a mean particle size of 205 ± 8 nm with a positive surface charge of 31.2 ± 5.3 mV (Fig. S2A), which can be attributed to the presence of polythyleneimine (PEI) imparting a positive surface charge to the particles. A particle size of approximately 200 nm makes both formulations desirable for tumor delivery by exploiting physiologically relevant enhanced permeation and retention (EPR) effect [40].

4.2.2. Evaluation of drug entrapment and loading efficiency of Erlo and QA in nano formulations

Amount of Erlo and QA entrapped in nanoparticles was estimated in lysed formulations using UPLC (Waters Inc., Milford, MA, USA) with established protocols. Erlo-NPs had Erlo entrapment of 26.8 ± 4.8% (4.5% drug loading; 2.49 mM drug concentration) and QA-NPs had QA entrapment of 31.8 ± 4.6% (5.3% drug loading; 6.72 mM drug concentration) (Fig. S2B).

4.2.3. In-vitro drug release studies for Erlo and QA from nano formulations

Fig. S2C represents the release profile for both formulations, reproduced from the already published individual nano formulation studies [31,32]. As can be seen that Erlo-NPs has a delayed Erlo release, as compared to QA from QA NP. For first 6 h, there was negligible Erlo release from the nanoparticles. QA showed an immediate release with 97.3 ± 2.3% release in the first 30 min. As discussed, Erlo-NPs demonstrated negligible release in the first 24 h followed by a gradual release of Erlo from nano formulations (~24% release in first 72 h). Such drastic release profiles of both nano formulations can be exploited to our advantage via a co-incubation nano therapy. Rapid QA release would sensitize cells prior to Erlo release, making the cancerous cells vulnerable to Erlo therapy. This sensitization technique of QA has been successfully reported to be effective in improving chemotherapeutic efficacy in various tumors [19,41]. TEM analysis confirmed spherical shape and morphology for both nanoparticle formulations (Figs. S2D and S2E). Surface morphology of developed particles and their release profiles were reproduced with permission from their respective publications.

4.3. Concurrent treatment with both formulations does not attenuate the ability of either of the delivery systems to be taken up by NSCLC cells

Nano delivery systems are formulated to improve the deliverability of drugs and other components to their desired site of action. Physicochemical characteristics of these tiny particles facilitate their transport across cell membrane, either through the GIT into systemic circulation, or from the systemic circulation to site of action. For injectable or inhalable formulations that are administered for NSCLC treatment, the most difficult barrier to cross is the tumorous cell membrane. We earlier reported that both developed formulations had significantly higher intracellular uptake as compared to plain QA and plain Erlo [31,32]. In this study, uptake of both particles was evaluated when administered

simultaneously, for a period of 3 h, to make sure either of them did not interfere with uptake of the other. Innate green fluorescence of QA was used to visualize uptake of QA-NPs, and Texas red (TR) dye was used as a substitute for Erlo to visualize Erlo-NPs. Fig. 2A indicates the intracellular uptake of TR along with plain QA, both separately and in combination, which serve as a control and signify the uptake of plain drug solutions. As can be seen, both TR and QA plain drug solution entered the cells and accumulated in the cytoplasm around the nucleus, but the fluorescence intensity was pretty weak. This indicates the inefficiency of plain drug solutions to travel intracellularly without a delivery system. On the other hand, Fig. 2B indicates the intracellular uptake of nano formulations for QA and TR. An enhanced fluorescence intensity can be seen in comparison to Fig. 2A with the same treatment conditions. This suggests the excellent potency of nano-formulations to be taken up by cancer cells. Furthermore, both green (QA) and red (TR) fluorescence was observed to be accumulating around the nucleus indicating that both particles were taken up by cells without much interference from the other particle. Fig. 2C is a zoomed in representation of a cell showing uptake of both nano-formulations. The arrows indicate excellent co-localization of both QA and Texas-red which were delivered intracellularly by efficient co-incubated nanocarrier systems. This premise is important in establishing that a combination of two nanoparticles can be successfully administered to cells without any interference issues.

4.4. Nano delivery systems for QA and Erlo enhance the synergistic potential of QA + Erlo drug therapy

Testing plain drug combinations established that sensitization of cells with QA prior to Erlo administration is essential for optimum synergy (Fig. 1). However, with nanoparticle therapy, the amount of drug available to show effect is contingent upon its release from the nanoparticle core. On evaluating drug release profile for both nanoparticles (Fig. S2C), it was understood that QA-NPs had a faster release of QA (97.3 ± 2.3% in 30 min) as compared to the delayed Erlo release from Erlo-NPs (with virtually no release in the first 6 h followed by gradual release after 24 h). Keeping the release profiles and the favorable pre-incubation strategy in mind, both nanoparticles were co-administered as treatment. Such a scenario will have QA released faster in cells than Erlo, resulting in desired cell sensitization, followed by delayed Erlo release, that would then have much more impact, resulting in a highly efficacious system. This hypothesis was backed by cell viability data, as seen in Fig. 3A which compares plain drug pre-incubation strategies with combinatorial nanoparticle treatment. Both drugs were combined at the previously established QA to Erlo ratio of 1:5, and it can be seen that at all combination concentrations, nanoparticle treatment was significantly more efficacious than plain drug combination strategies with lower values of cellular viability; QA 0.37- and Erlo 1.8 μM: 54.7 ± 11.5% cell viability for pre-incubation versus 41.6 ± 5.7% for nanotherapy ($p < 0.05$ for pre-incubation versus nanotherapy); QA 0.78- and Erlo 3.75 μM: 54.1 ± 6.6% cell viability for pre-incubation versus 36.6 ± 3.9% for nanotherapy ($p < 0.0001$ for pre-incubation versus nanotherapy); QA 1- and Erlo 5 μM: 47.1 ± 1.8% cell viability for pre-incubation versus 27.9 ± 0.4% for nanotherapy ($p < 0.0001$ for pre-incubation versus nanotherapy). As discussed previously, this enhanced efficacy of nanotherapy can be attributed to higher cellular internalization of nanoparticles resulting in higher accumulation of drugs in cellular micro-environment.

Synergy between the two drugs was evaluated by calculating the combination indices (CI) calculated at ED_{50} values for all treatment groups as per chou-talalay method [42] indicating successful synergy (Fig. 3B). CI for pre-incubation of QA + Erlo Solution (1 μM and 5 μM) was found to be 0.6485 (Fig. 3B). CI for nano formulations was calculated in a similar way and this index was compared to pre-incubation CI. For QA + Erlo NPs: 1 μM + 5 μM treatment group, the combination index was found to be 0.2536. As seen in Fig. 3B, nanoparticle combination yielded the lowest value for CI, indicating an expressively higher synergy compared to pre-incubated plain drug solutions. With low cell viability and CI values, combination concentration ratio of QA + Erlo: 1 μM + 5 μM was selected for all further experimental studies.

4.5. Combination nanotherapy successfully inhibits colony formation in NSCLC cells: clonogenic assay

Surgical resection of tumor often results in an incomplete eradication

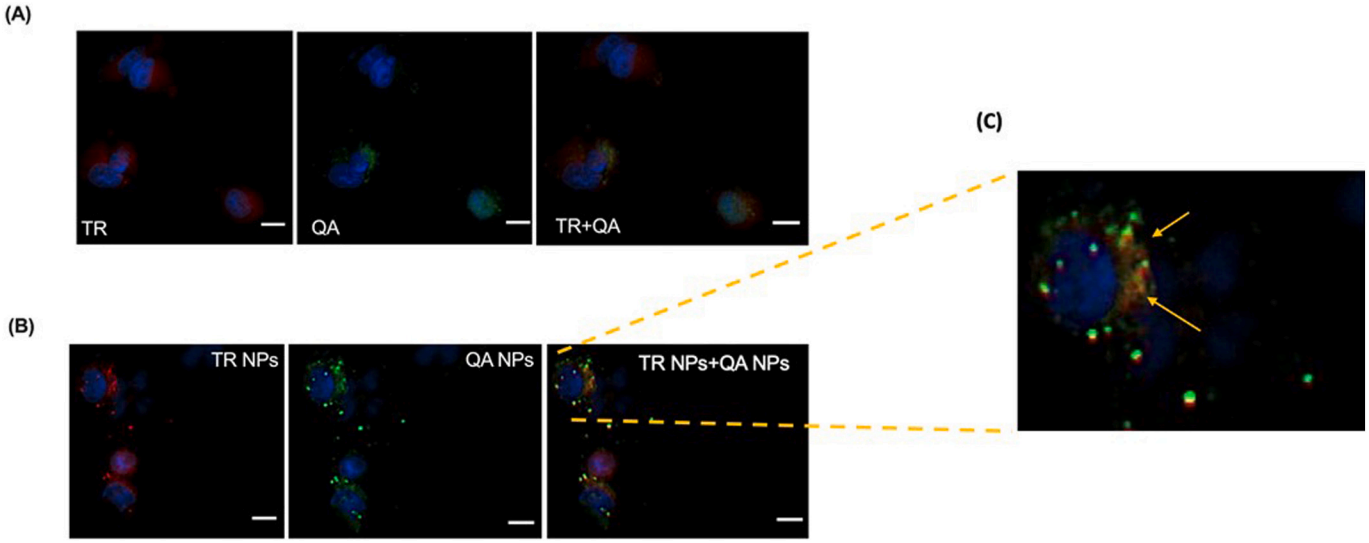

Fig. 2. (A) Cellular uptake study indicating cellular internalization for Texas red dye (TR) (simulating Erlo in NPs) and plain QA (innate green fluorescence) in A549 cells after 3 h of treatment. Nucleus is stained blue with DAPI. Both TR and QA are internalized in cells when administered together and are not interfering with each other with respect to cellular internalization, as seen by from the TR + QA. (B) Cellular uptake study for combination NPs using A549 cells. Treatment was done for 3 h and both QA-NPs and Texas Red-NPs (TR NPs) were co-administered. It can be clearly seen that none of the two particles interfered with internalization of the other, as can be seen from the figure. This reveals that nanoparticles can be co-administered without interference as a combinatorial therapy. (C) Zoomed-in representation of intracellular uptake of nano formulations of Texas red and QA indicating co-localization of both nano formulations in the cytoplasm around the nucleus. Scale bar 40 μm. These images are representative of an experiment with 3 replicates ($n = 3$). (For interpretation of the references to color in this figure legend, the reader is referred to the web version of this article.)

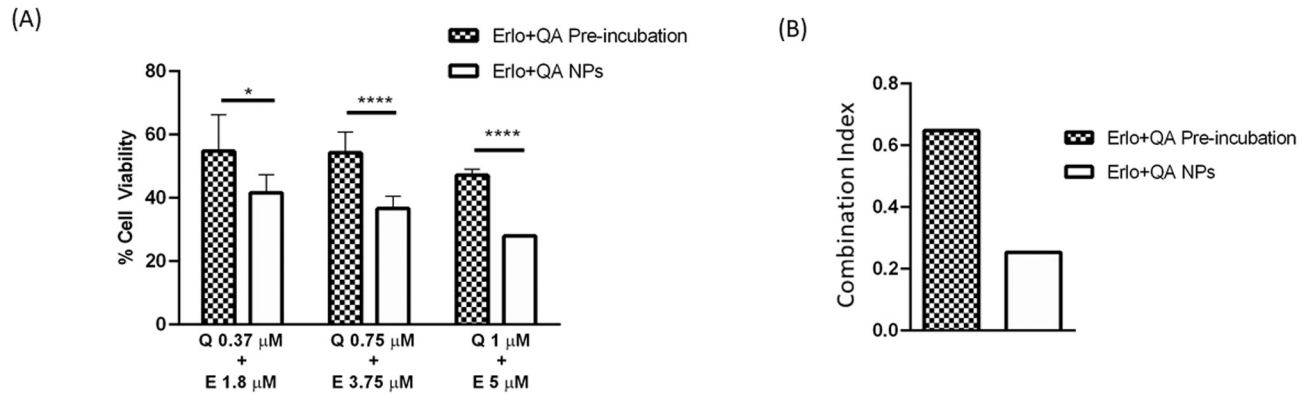

Fig. 3. (A) Represents cytotoxicity data comparing nanoparticle combination and drug solution combinations. A significant difference between viabilities for combination nanoparticles treatment and plain drug combination can be seen, indicating higher therapeutic value for nano engineered delivery system. (B) Plot represents combination index for pre-incubation strategy along with CI for nano engineered systems. Lower CI values indicate higher synergy. Data are presented as % cell viability and represent mean ± SD (average of 3 individual experiment with n = 6) (*$p < 0.05$, **$p < 0.01$, *** $p < 0.001$, **** $p < 0.0001$).

of tumor and a small number of cancerous cells remain viable physiologically which may then relapse into a tumor via formation of colonies at distant organs. A successful inhibition of such colonies can suggest that the proposed combination therapy not only helps in treatment of NSCLC but also serves as a maintenance therapy post tumor eradication. To study this situation in-vitro, a clonogenic assay was performed which involves starting with a small number of cells (500/well) in 6-well TC treated plates and allowing longer incubation and colony formation. In this assay, A549 cells were treated with QA (1 μM), Erlo (5 μM), QA + Erlo (1 μM + 5 μM) solution and QA + Erlo NPs (1 μM + 5 μM). As can be seen from Fig. S3A, NP combination significantly inhibited the formation of colonies as compared to control, QA alone and Erlo after treatment for 48 h. Relative to control, 1 μM QA had 93.7 ± 3.8% colony growth and 5 μM Erlo had 70.5 ± 6.5% colony growth. QA + Erlo solution had 46.4 ± 3.5% colony growth as compared to control whereas NPs combination had a 39.4 ± 3.8% colony growth relative to the control (Fig. S3B). Although a visible (Fig. S3A) and numerical (Fig. S3B) difference could be seen, difference in colony growth reduction between QA + Erlo and NP treated groups wasn't quite statistically significant ($p = 0.0693$), which could be due to limited sample size for the experiment. In addition, it is hypothesized that in-vivo translation would bring out the true potential of delivery system and a significant difference may be visible which can be attributed to enhanced uptake of nano delivery systems as compared to plain drugs in physiological tumor tissues.

4.6. Combination nanotherapy successfully attenuates progression of tumor growth in simulated 3D-cell based NSCLC model

4.6.1. Visual estimation

Among the multiple analytical methods used to analyze the efficacy of our proposed combinatorial therapy on 3D spheroidal structure, the primary assessment was done via a visual estimation of spheroids using an inverted microscope. This type of assay gives quantifiable results about the extent of spheroid size reduction over a period of 15 days. Following a 3-day incubation period to attain sturdy spheroidal structures, spheroids were dosed with QA (1 μM), Erlo (5 μM), QA + Erlo (1 μM + 5 μM) solution and QA + Erlo NPs (1 μM + 5 μM) in two ways; a single dose set where spheroids received treatments on day 0 of the study; and a multiple dose set where the spheroids received treatments after every 72 h up to 15 days. Spheroid images were taken at each dosing interval (or every 72 h for single dose spheroids) to track spheroid growth inhibition. As can be seen from Fig. 4A & B, tumor volumes for both single and multiple dose spheroids treated with combination solution and combination nanoparticles showed higher growth inhibition as compared to control and QA treated spheroids. Erlo treated spheroids also showed similar growth inhibition for both type of dosing but overtime, as discussed earlier, Erlo treated cells may mutate to acquire resistance.

Single Dose Spheroids: In-depth visual analysis yielded the following sizes for spheroids at each time point for single dose studies: Day 0 - Control: 2.5 ± 0.2 mm^3, QA: 2.4 ± 0.3 mm^3, Erlo: 2.6 ± 0.4 mm^3,

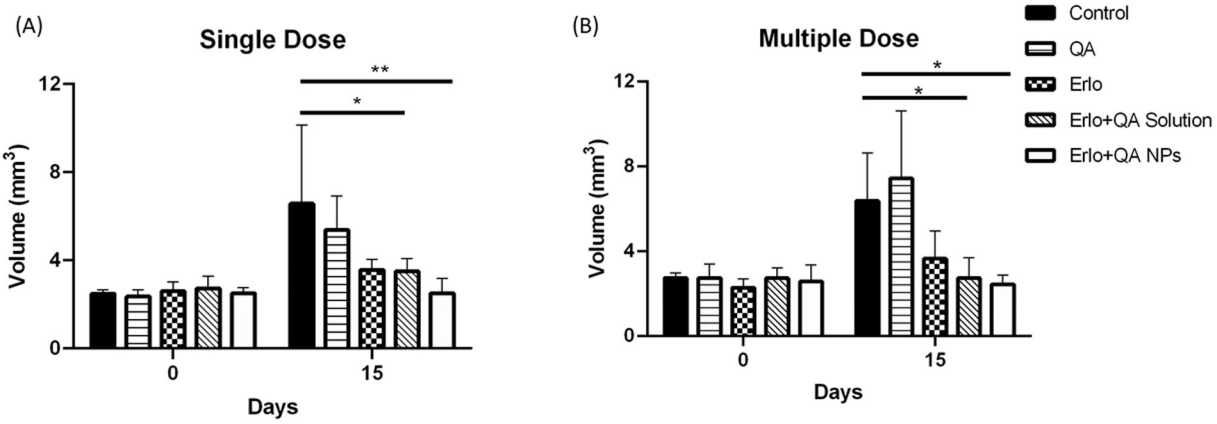

Fig. 4. (A) and (B) Plots represent spheroid volumes plotted for Single dose and Multiple dose treatments for A549 spheroids. A significant difference can be seen at the end of study between combination solution and combination NPs for single dose treatment. Data represents mean ± SD (n = 6) (*$p < 0.05$, **$p < 0.01$, *** $p < 0.001$, **** $p < 0.0001$), compared between treatment and control groups, as indicated.

QA + Erlo Solution 2.7 ± 0.6 mm^3, and QA + Erlo NPs 2.5 ± 0.3 mm^3. This indicates that all spheroids had similar sizes on day 0, i.e. prior to treatment. Day 3 sizes were as follows - Control: 3.3 ± 0.4 mm^3, QA: 4.4 ± 0.5 mm^3, Erlo: 3.0 ± 0.3 mm^3, QA + Erlo Solution 3.0 ± 0.2 mm^3, QA + Erlo NPs 2.9 ± 0.5 mm^3 (*Data not shown*). After 15 days, control spheroids had an average volume of 6.6 ± 3.6 mm^3 (2.64-fold growth as compared to its volume on day 0), whereas QA + Erlo NPs treated spheroids had an average volume of 2.5 ± 0.7 mm^3 (0-fold increase in spheroid volume in comparison to its volume on day 0). QA + Erlo solution treated spheroids had a volume of 3.5 ± 0.6 mm^3 ($p < 0.05$; a 1.29-fold increase in spheroid volume as compared to its volume on day 0), Erlo treated spheroids had an average volume of 3.6 ± 0.5 mm^3 (a 1.38-fold increase in spheroid growth as compared to its volume on day 0) and QA treated spheroids had an average volume of 5.4 ± 1.5 mm^3, a 2.25-fold increase in spheroid volume as compared to its size on day 0 (Fig. 4A). Visual representation for singly dosed spheroids reveal that groups treated with nano formulation had no change in their average volume from day 0 to day 15 whereas all other treated spheroid groups showed a certain degree of increase in their volume as compared to their volumes on day 0, i.e. prior to treatment.

Multiple Dose Spheroids: Similar trends were observed for multiple dose sets, although, no significant difference was observed in spheroid size between combination solution treated spheroids and combination NPs treated spheroids. Day 0 - Control: 2.7 ± 0.2 mm^3, QA: 2.7 ± 0.7 mm^3, Erlo: 2.3 ± 0.4 mm^3, QA + Erlo Solution 2.7 ± 0.5 mm^3, QA + Erlo NPs 2.6 ± 0.8 mm^3. Day 3 sizes were as follows - Control: 4.0 ± 0.3 mm^3, QA: 4.0 ± 0.5 mm^3, Erlo: 3.0 ± 0.3 mm^3, QA + Erlo Solution 2.6 ± 0.7 mm^3, QA + Erlo NPs 2.5 ± 0.5 mm^3. At day 15, following measurements were observed - Control: 6.4 ± 2.3 mm^3, QA: 7.4 ± 3.2 mm^3, Erlo: 3.6 ± 1.3 mm^3, QA + Erlo Solution 2.7 ± 1.0 mm^3, QA + Erlo NPs 2.4 ± 0.4 mm^3 (Fig. 4B). As can be seen, while average tumor volume for NP treated group was lower than plain drug combination group, no significant difference was observed. This can be attributed to the fact that effectiveness of combination therapy is contingent of delayed Erlo release from NPs, and a multiple dosing regimen may disrupt the release profiles and hence may not accurately represent the availability of both drugs to the cells. In such a scenario, combination solution too shows similar effect to combination NPs due to high drug availability. In addition, the 2D size measurement does not necessarily reflect the composition and build-up in 3-dimensional tumor core, for which we performed live/dead and 3D cell viability assays, as discussed in the next section.

In summary, our results indicate that QA + Erlo NPs can provide significant improvement in tumor reduction at a lower dosing frequency

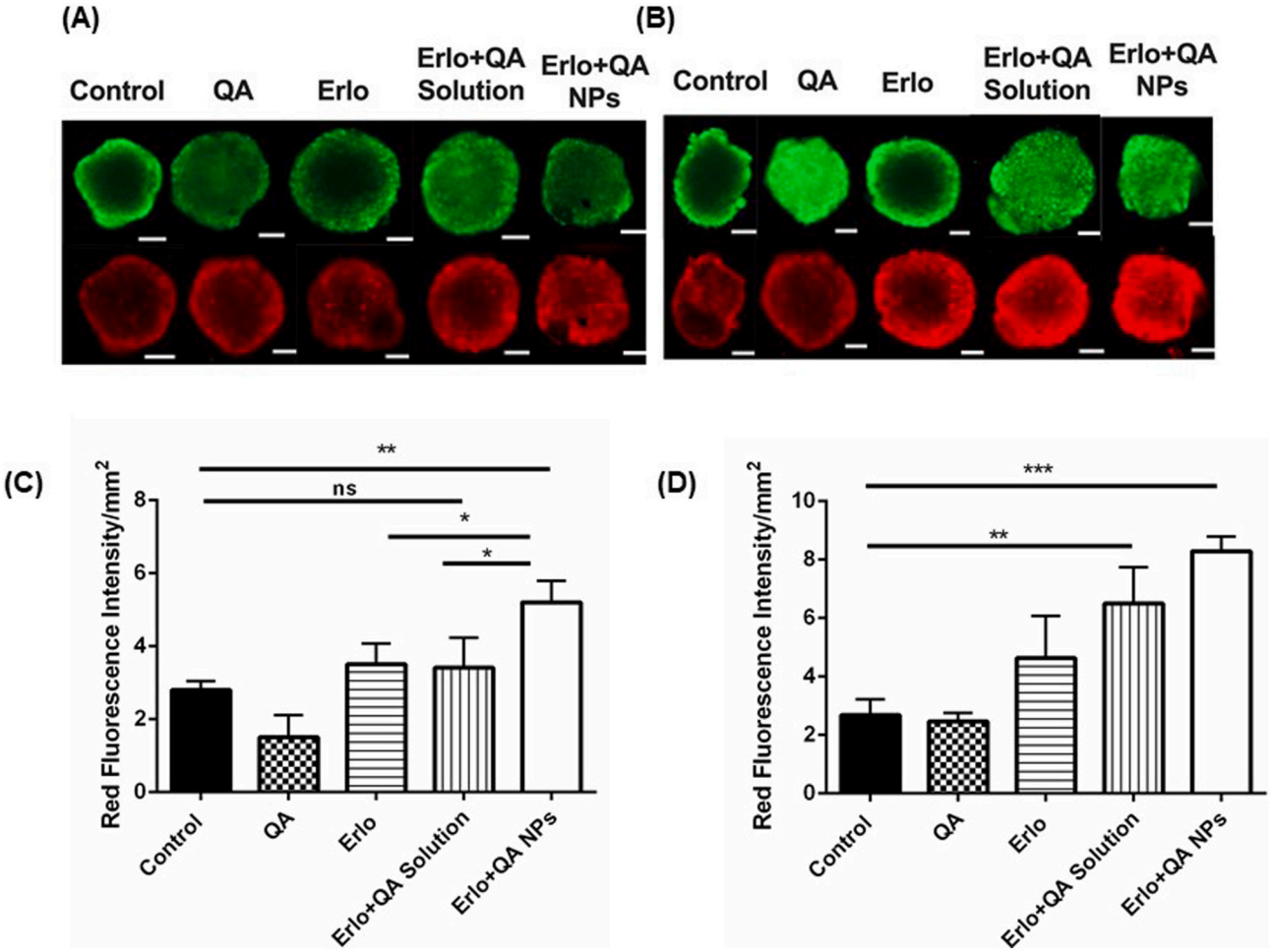

Fig. 5. (A) & (B) Representation of Live/Dead cells in the spheroid mass. Live cells are stained green and dead cells are stained red using a live/dead cell assay kit. Simple visual measurement of spheroid size can be misleading as it does not account for live or dead cells in the spheroid mass. Keeping that in mind, live/dead assay provides a higher degree of analysis for determining the efficacy of nano formulations in 3D spheroidal structure. (C) & (D) Plots represent red fluorescence intensity/mm^2 for single dose and multiple dose regimen. A significantly higher red fluorescence intensity can be seen for combination solution and combination NPs for single dose spheroids indicating higher portion of dead cells. Similar trend can be seen for multiple dose regimen, but it lacks significance. Data represents mean ± SD (n = 6), $*p < 0.05$, $**p < 0.01$, $***p < 0.001$, $****p < 0.0001$, compared between treatment and control groups, as indicated, Scale bar 100 μm. (For interpretation of the references to color in this figure legend, the reader is referred to the web version of this article.)

in preclinical and clinical settings. Figs. S4 & S5 indicate representative images of spheroids treated with single dose and multiple dose therapy respectively.

4.6.2. Live/dead 3D-spheroid assay

While physical measurement of spheroid size gives a brief idea about the treatment efficacy, it may not reveal the state of cells within the spheroid mass, i.e. whether there are dead/necrotic cells in the tumor core. Thus, to have a clearer picture about treatment efficacy, it is important to visualize cell viability in a spheroid mass. This was done using a live/dead assay kit (Biotium, Fremont, CA, USA), which stained the live cells green and dead cells red. As can be seen in Fig. 5A & B, the intensity of red fluorescence is the least for control group spheroids and maximum for combination NPs in both single dose (Fig. 5A) and multiple dose (Fig. 5B) spheroids, indicating more dead cells for NPs treated spheroids. This red fluorescence intensity/mm^2 (RFI/area) can be quantified, as seen in Fig. 5C & D for single and multiple dosing respectively. For single dose, RFI with respect to area (RFI/mm^2) for nanotherapy was found to be 5.2 ± 0.6 units, which was significantly higher than the RFI/mm^2 calculated for combination solution (3.4 ± 0.8, $p < 0.05$) and control spheroids (2.8 ± 0.2, $p < 0.01$). On the other hand, for multiple dose, although RFI/mm^2 was higher for nanotherapy (8.3 ± 0.5) than combination solution (6.5 ± 1.2), no significant difference was observed between the two groups, which can be attributed to multiple dosing, as explained earlier. Although, there was a significant difference observed between nano therapy and control (2.68 ± 0.53, $p < 0.001$) and combination solution and control as well ($p < 0.01$).

4.7. Combination nanotherapy results in a G0-G1 cell cycle arrest for NSCLC cells with low cell population in G2-M phase

Previous reports suggest that both Erlo-NPs and QA-NPs arrest cells in apoptotic phase and thus it was important to evaluate the cell cycle arrest pattern with the combination of both particles [31,32]. Cell cycle analysis was performed using BD Accuri™ C6 (BD Biosciences, San Jose, CA, USA). Fig. S6A indicates the population of cells in various stages of the cell cycle i.e. G0-G1 phase, S phase and G2-M phase. Post G2-M phase, the cells differentiate into daughter cells and divide. Plot representing cell cycle (Fig. S6B) reveals that population of QA + Erlo NPs treated cells was significantly higher in G0-G1 phase (90.7 ± 1.4%) as compared to control (78.6 ± 6.1%) ($p < 0.05$). There was no significant difference in cells in S phase. G2-M phase had the least population of cells for QA + Erlo NPs treated cells (4.5 ± 1.9%) which was significantly lower than cell population for control cells (15.3 ± 5.4%) ($p < 0.05$). No significant difference was observed between QA + Erlo solution (5.7 ± 1.1%) with respect to control (Fig. S6B). Thus, it can be hypothesized that cells are arresting in G0-G1 phase along with apoptotic phase which can be indicated by quantification of apoptotic marker caspase-3, discussed in later sections.

4.8. Combination nanotherapy results in inhibition of autophagy process

A549 cells were used to test the effect of all treatments on autophagy inhibition which was evaluated by fluorescent staining of the membrane protein LC3B-II. Increase in green fluorescence intensity signifies higher accumulation of LC3B-II, hinting at more intermediate autophagosomes rather than autolysosomes and ATP. The in-vitro assay was performed using CYTO-ID® Autophagy Detection Kit (Enzo Life Sciences Inc., Farmingdale, NY, USA). As seen in Fig. S7A, fluorescence intensity was high for QA treated cells (2.0 ± 0.6 times control) and combination NPs treated cells (2.0 ± 0.6 times the control), whereas the intensity for Erlo treated cells was similar to control group indicating no autophagy inhibition in these group of cells. Although inhibition extent was higher in combination NPs as compared to combination solution (1.8 ± 0.2 times control), the difference was not found to be statistically significant.

4.9. Combination nanotherapy enhances expression of caspase-3, indicating successful apoptosis in NSCLC cells

Erlo has been reported to induce apoptosis in cancer cells, which is also its proposed mechanisms to inhibit cancer progression [43]. QA on the other hand is reported to induce apoptosis and inhibit autophagy, as discussed in the earlier section [19,21]. Caspase-3 is an identified marker for apoptosis, and induction of caspase-3 is a reliable marker for apoptotic induction. Caspase-3 levels were evaluated in-vitro in A549 cells using EnzChek® Caspase-3 assay kit. A549 cells were treated with QA (1 μM), Erlo (5 μM), QA + Erlo (1 μM + 5 μM) solution and QA + Erlo NPs (1 μM + 5 μM). QA treatment resulted in a fluorescence which was 2.3 ± 1.3 times higher than control, Erlo treatment resulted in a 2.2 ± 1.3 times higher fluorescence than control, combination solution resulted in a 2.3 ± 1.0 times higher intensity than control and combination nanotherapy resulted in a 3.2 ± 1.6 times higher fluorescence than the control cells. All treatment groups exhibited high fluorescence intensity relative to the control and there was no significant difference between the treatment groups, although, combination NPs exhibited higher levels of fluorescence indicating higher caspase-3 levels (Fig. S7B).

4.10. Combination nanotherapy markedly affects the expression levels of autophagy marker LC3B along with effect on NF-κB

As described earlier, LC3B-II is over-expressed in event of autophagy inhibition [44]. This overexpression was tested using western blotting. Another marker that was tested was NF-κB, responsible for DNA transcription and overall cell survival. Inhibition of this marker will indicate lack of DNA transcription and thus less probability of cell survival. Fig. S7C & E represent the blots obtained from A549 cells after 24-h treatment with QA (1 μM), Erlo (5 μM), QA + Erlo (1 μM + 5 μM) solution, and QA + Erlo NPs (1 μM + 5 μM). As seen in Fig. S7C, LC3B-II was found to be significantly upregulated with QA + Erlo NP treatment. On densitometric analysis, normalized band intensity (LC3B-II) for combination NPs group was found to be significantly higher than control group and Erlo treated cells (0.5 ± 0.2 versus 0.1 ± 0.03 and 0.1 ± 0.02, respectively), depicting a 5-fold increase in LC3B-II accumulation (Fig. S7D).

The downregulation of NF-κB can be visualized for both QA + Erlo solution and QA + Erlo NPs (Fig. S7E) as compared to control cells and even as compared to QA and Erlo treated cells. Intensity for NF-κB bands, as seen in Fig. S7F, was significantly lower for combination NPs treated cells, as compared to QA treated cells (0.4 ± 0.07 versus 0.9 ± 0.05, respectively; $p < 0.05$). In addition, QA + Erlo solution too showed significant reduction in NF-κB levels as compared to QA treated cells (0.4 ± 0.18 vs 0.9 ± 0.05, respectively; $p < 0.05$). However, no significant difference was observed between QA + Erlo solution and QA + Erlo NPs (Fig. S7F).

4.11. Combination nanotherapy successfully induces LC3B-II and inhibits NF-κB levels in a 5D-sphericalplate based model

As discussed in the previous section, Erlo and QA both affected the regulation of certain molecular markers expressed in certain events like autophagy (LC3B-II). Apart from these, certain markers like NF-κB are essential for cell survival via regulation of DNA transcription. So far, it has been established that combination NPs therapy upregulates autophagic marker LC3B-II, indicating an inhibition in autophagy and downregulates NF-κB thus shunting DNA transcription and overall cell survival. The previous molecular marker evaluations were carried out on 2D layer of cells, which, as discussed in previous sections, may not represent physiological 3-dimensional tumor growth and progression, and thus tumor penetration and efficacy. To simulate physiological conditions while studying molecular markers, a 3D spheroid model was utilized. To extract enough protein, many identical spheroids were

grown in a specially designed 5D-Sphericalplate (Kugelmeiers, Switzerland). This specially designed plate can accommodate up to 9000 spheroids/plate i.e. 750 spheroids/well. This high number of spheroids facilitate high protein extraction levels, essential to accurately evaluate expression levels of molecular markers. A typical well of this specially designed plate is seen in Fig. 6A. Expression levels were evaluated using western blot technique as described in earlier section. Both LC3B-II and NF-κB were tested. As seen in Fig. 6B, expression levels align with 2D cell-based models. Band intensities were measured and normalized, as done for 2D western blots and as seen from Fig. 6C, expression levels for LC3B-II in nanotherapy treated group were higher (0.8 ± 0.2) as compared to QA (0.3 ± 0.2), Erlo (0.5 ± 0.3) and combination solution (0.5 ± 0.1) therapy. On the other hand, expression levels for NF-κB were lower for nanotherapy (0.3 ± 0.1) and combination solution treatment (0.2 ± 0.1) as compared to QA (0.8 ± 0.1), Erlo (0.6 ± 0.2) ($p < 0.05$). It can be inferred that in a simulated 3D tumor model, a trend was seen for expression levels of all tested proteins, similar to that observed for 2D cell-based model testing.

5. Discussion

Erlo is a first-generation EGFR tyrosine kinase inhibitor, used for NSCLC therapy and was approved as oral tablets by the FDA in 2004 (Tarceva®). Although potent, Erlo has been widely criticized for development of acquired drug resistance (ADR) in patients over chronic exposure [45,46]. ADR development in NSCLC can be attributed to genetic mutations in cells at specific amino acid residues. EGFR mutations have been explored in detail and it has been inferred that KRAS (Kirsten Rat Sarcoma viral oncogene homolog) mutations are the primary source of ADR while T790M mutation (replacement of methionine in place of threonine at the 790th amino acid position on the EGFR domain) is cited as a secondary and the most aggressive source of resistance [47]. Irrespective of the primary or secondary source of mutation, it has been revealed that usually some form of ADR is developed within 10 months of Erlo therapy [47]. This renders one of the most potent molecules for NSCLC therapy futile. One of the go-to approaches to rescue such potent molecules from going out of clinics is to come up with a combinatorial therapy alongside a molecule capable of either reversing the ADR or sensitizing the cells enough for effective therapy [22,48]. One such attempt to improve Erlo therapy and delay ADR further was made by Dermawan et al.. The group aimed to combine Erlo with Quinacrine (QA), a widely approved anti-malarial drug [22]. Prior to development of Erlo-QA combination, QA was reported to be a potent chemotherapeutic agent in multiple cancers such as breast and colon cancer [49,50];

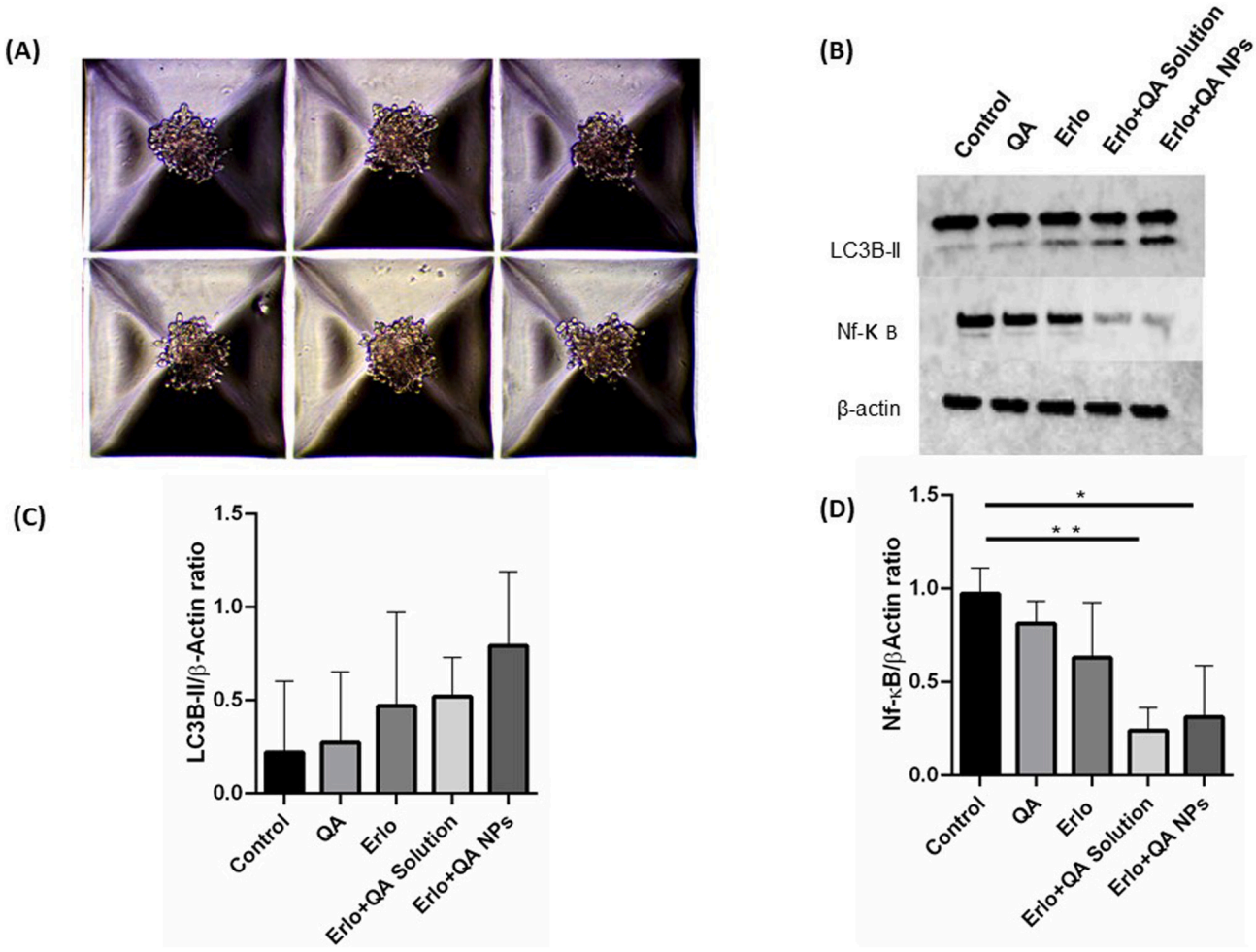

Fig. 6. (A) Figure represents placement of A549 cell spheroids in a 5D-Sphericalplate. Each plate contains about 9000 spheroids with a configuration of 750 spheroids/well. (B) Western blots representing expression levels for LC3B-II and NF-kb along with ß-Actin levels. The results align with those obtained from 2D cell models and indicate that LC3B-II levels are upregulated for combination NPs as compared to other treatment groups, indicating inhibition of autophagy and NF-kb levels are downregulated for combination NPs as compared to other treatment groups hampering chances of cell survival and DNA transcription. (C) and (D) Plots represent normalized band intensities for LC3B-II and NF-kb respectively. A slight increase in regulation of LC3B-II can be seen for combination NPs as compared to other treatment groups, although non-significant. A significant decrease in expression level of NF-kb can be seen for combination NPs treated cells as compared to control group of cells. Data represents mean ± SD (n = 3) (*$p < 0.05$, **$p < 0.01$, *** $p < 0.001$, **** $p < 0.0001$).

and was reported to work via induction of apoptosis. Apart from this, multiple reports also suggested that QA could be a universal chemotherapeutic adjuvant due to its chemo-sensitization effects in multiple cancers [51,52]. These revelations about QA prompted its use as an adjuvant to Erlo in an attempt to treat NSCLC. Studies by Dermawan et al. revealed that QA sensitizes cells for Erlo chemotherapy via inhibition of FACT complex (facilitates chromatin transcription) subunit SSRP1 and via an inhibitory effect on NF-κB. QA adjuvant therapy also inhibited cell cycle progression in NSCLC and overall QA was reported to reverse Erlo induced ADR in-vitro. These promising in-vitro studies led to Phase-I clinical trials of this adjuvant therapy, conducted by Bhateja et al. The clinical study successfully established the maximum tolerated dose for QA (50 mg) and Erlo (150 mg) every alternate day. Although only 10 patients enrolled in this study, most of them either had continued disease progression or partial response. Hence the study concluded limited efficacy of combinatorial therapy in improving NSCLC progression. [23].

This unsuccessful development may be attributed to overall toxicity, biodistribution or even lack of therapeutic efficacy physiologically. Nano drug delivery systems are known to enhance the therapeutic effects of a drug by increasing its availability specifically at the site of action and by increasing the cellular internalization as compared to plain drugs [53]. PLGA is one of the most widely used biodegradable polymer that has been utilized for fabrication of polymeric nanocarriers. It has a glass transition temperature between 37 °C–40 °C which makes its relevant for physiological use [54]. The ratio of lactic acid and glycolic acid is an important factor to consider while tailoring the release profile for any drug. Use of a 50:50 ratio has been demonstrated to be responsible for a fast and efficient drug release from a glassy polymeric matrix at physiological conditions [38]. Nanoparticles made using PLGA were shown to have high tissue penetration, attributed to their favorable size and surface charge [55]. Once in tumor tissue, efficacy of the therapy depends on the ability of nano-formulation to cross cell membrane barrier and enter the cells where potent drug can be released to show efficacy. Despite these stellar advantages, utility of nanocarriers in clinical applications has been limited due to safety concerns and limited efficacy in comparison to plain drug therapy. However, recent advances in development of polymeric nanoparticles have led to the consensus that safe and efficacious delivery of polymeric nanocarriers is indeed viable for cancer therapeutics. A Phase-II clinical study by Ranade et al. demonstrated excellent utility of paclitaxel-loaded polymeric nanoparticles for breast cancer treatment. Authors reported excellent safety profile and enhanced therapy in comparison to plain paclitaxel [56]. This study encouraged us to develop two polymeric nanoformulations, as previously reported [31,32] to try and better the effects of Dermawan et al. The development process was done in two steps. First step involved fabrication of optimized formulations for both drugs and studying their extensive in-vitro therapeutic behavior in comparison to plain drug solutions. Erlo was loaded on PLGA polymeric matrix as a cyclodextrin complex to tackle solubility issues [31]. QA on the other hand was developed as a polymeric nano formulation with a positive surface charge imparted using polyethyleneimine (PEI) [32]. Both formulations were recently reported to have enhanced cytotoxic efficacy as compared to drug solutions [31,32]. Drug release profiles for both formulations revealed that QA formulation had an immediate release compared to a delayed release for Erlo nanoformulation (Fig. S1). The second step involved synergistic testing of two developed formulations and testing their efficacy in bio-relevant cellular models, as reported in this study. The extent of synergy was evaluated by computing the combination indices. Dermawan et al. reported a CI for Erlo:QA (5:1) to be 0.81. This was confirmed in our study as we report a combination index of 0.8525. We further proposed that sensitizing cells with QA prior to Erlo administration may lead to an enhanced therapy. That hypothesis was confirmed via computing CI for Erlo:QA (5:1) where QA was administered in cells 6 h prior to Erlo treatment. The CI reduced to 0.64, indicating stronger synergism. Further, nanoformulations were incubated with cells simultaneously and the varied release profiles of both formulations resulted in an immediate QA release and delayed Erlo release, which fits the pre-incubation hypothesis perfectly. The CI calculated for nano formulations was 0.25, which was significantly lower than previously reported CIs for plain drug solutions. Lower values of CI indicate stronger synergy between two nanoformulations, as compared to plain drug solutions.

However, revelation of excellent synergy between drug-loaded nanoformulations is not sufficient to move on to pre-clinical testing and extensive in-vitro testing needs to be done for appropriate dose selection for animals along with validation of efficacy on multiple cell-based models. However, there has been a huge gap between in-vitro and in-vivo testing in terms of efficacy. Therapies showing excellent in-vitro efficacy have often failed to translate their potency in animals or humans. This failure can be attributed to the fact that in-vitro models fail to mimic physiological conditions. The major constraint occurs in cell-based models as most of the in-vitro cell-based models are two dimensional (2D), whereas physiological tumors are complex multi-layered three-dimensional (3D) structures. This complex multifaceted structure of physiological tumors poses a lot of resistance for drug penetration with often uneven distribution of therapy across the tumor. A more accurate way of replicating physiological tumor conditions is by actually growing a 3D tumor in-vitro. Simulating a 3D cell-based tumor model in-vitro can also aid in more accurate identification of dose as well as help with high throughput screening of drug dose [57]. This 3D model can not only be used for gauging the therapeutic efficacy, but also to study protein expression at a molecular level. Such molecular studies on a 3D spheroid would require multiple spheroids grown in exactly same conditions to yield enough protein for appropriate quantification. However, growing multiple spheroids separately may lead to variations in protein expression levels. A recently developed 5D-Sphericalplate (Kugelmeirs, Erlenbach, Switzerland) circumvents this issue of variation by allowing a bulk growth of spheroids in a single well with a capacity of 750 spheroids in a single well. Recently, Wassmer et al. demonstrated the utility of 5D-Sphericalplates in extracting higher amounts of insulin in comparison to conventional methods of spheroid formation. In comparison to a petri-dish method, drop method and a mold method, 5D-Sphericalplates generated more amount of total protein, which will be essential for experiments requiring higher protein content [58]. Thus, a therapeutic efficacy evaluation and a molecular protein expression evaluation using a physiologically relevant model such as 3D Cell based assay makes our combinatorial therapy much more likely to not face efficacy related issues in pre-clinical studies.

6. Conclusion

The present study successfully demonstrates the utility of nanoformulations of Erlo and QA as a synergistic therapy for NSCLC treatment. Successful synergy was established between the two nanoformulations, indicated by low CI values (0.25 for nanoformulations versus 0.64 and 0.85 for plain drug solutions with and without QA sensitization prior to Erlo treatment, respectively). Apart from strong synergy, nanoformulations also exhibited satisfactory efficacy in bio-relevant tumor models involving 3D Spheroids. Moreover, nanoformulations showed satisfactory effects on molecular protein expression performed on a 5D-Sphericalplate; and inhibitory action on NF-κB was confirmed in the 5D model, deemed to be an important pathway for QA in sensitizing cells prior to Erlo treatment. Although some effects on molecular pathways may not be significantly different for nano formulations versus plain drug combination, it is very vital to note that optimum synergy can only be obtained with pre-sensitization of cells with QA prior to Erlo treatment. Such conditions are very difficult to mimic physiologically without a drug delivery system which is capable of tailoring drug release at the specific site of action. Thus, from a translational point of view, development of a nano combinatorial therapy is more viable than plain drug combination. Strong in-vitro

testing on bio-relevant models in this study has laid a platform to launch pre-clinical and clinical studies in the near future and this combinatorial therapy shows promise to be a potential frontline therapy to tackle NSCLC.

CRediT authorship contribution statement

Nishant S Kulkarni, MS; Conceptualization, Methodology, Validation, Investigation, Execution, Formal analysis, Writing – original draft, Software.

Bhuvaneshwar Vaidya, PhD; Conceptualization, Methodology, Validation, Investigation, Execution, Formal analysis, Software.

Vivek Gupta, PhD; Conceptualization, methodology, Writing – review and editing, Supervision, Project administration, Funding acquisition, Resources.

Declaration of competing interest

The authors declare no conflict of interest.

Acknowledgments

This study was supported by start-up funds provided to VG by College of Pharmacy and Health Sciences (CPHS), St. John's University; and School of Pharmacy, Keck Graduate Institute. NSK was supported by research assistantship provided by an NIH Research Enhancement Award (R15), 1R15HL138606-01A1 to Dr. Vivek Gupta.

Both NSK and BV contributed equally to the work.

Appendix A. Supplementary data

Supplementary data to this article can be found online at https://doi.org/10.1016/j.msec.2021.111891.

References

[1] H. Yu, Y. Wang, S. Wang, X. Li, W. Li, D. Ding, X. Gong, M. Keidar, W. Zhang, Paclitaxel-loaded core-shell magnetic nanoparticles and cold atmospheric plasma inhibit non-small cell lung cancer growth, ACS Appl. Mater. Interfaces 10 (2018) 43462–43471, https://doi.org/10.1021/acsami.8b16487.

[2] E. Brambilla, A. Gazdar, Pathogenesis of lung cancer signalling pathways: roadmap for therapies, Eur. Respir. J. 33 (2009) 1485–1497, https://doi.org/10.1183/09031936.00014009.

[3] S. Ekman, M.W. Wynes, F.R. Hirsch, The mTOR pathway in lung cancer and implications for therapy and biomarker analysis, J. Thorac. Oncol. 7 (2012) 947–953, https://doi.org/10.1097/JTO.0b013e31825581bd.

[4] F.G. Haddad, H.R. Kourie, J. Kattan, Targeting EGFR mutation in non-small-cell lung cancer: challenges and future perspectives, Future Oncol. 13 (2017) 201–204, https://doi.org/10.2217/fon-2016-0325.

[5] J.-K. Dong, H.-M. Lei, Q. Liang, Y.-B. Tang, Y. Zhou, Y. Wang, S. Zhang, W.-B. Li, Y. Tong, G. Zhuang, L. Zhang, H.-Z. Chen, L. Zhu, Y. Shen, Overcoming erlotinib resistance in EGFR mutation-positive lung adenocarcinomas through repression of phosphoglycerate dehydrogenase, Theranostics. 8 (2018) 1808–1823, https://doi.org/10.7150/thno.23177.

[6] M.H. Cohen, J.R. Johnson, Y.-F. Chen, R. Sridhara, R. Pazdur, FDA drug approval summary: erlotinib (Tarceva) tablets, Oncologist. 10 (2005) 461–466, https://doi.org/10.1634/theoncologist.10-7-461.

[7] U.S. Food & Drug Administration, Erlotinib (Tarceva), (n.d.). https://www.fda.gov/drugs/resources-information-approved-drugs/erlotinib-tarceva.

[8] W. Pao, V.A. Miller, K.A. Politi, G.J. Riely, R. Somwar, M.F. Zakowski, M.G. Kris, H. Varmus, Acquired resistance of lung adenocarcinomas to gefitinib or erlotinib is associated with a second mutation in the EGFR kinase domain, PLoS Med. 2 (2005), e73, https://doi.org/10.1371/journal.pmed.0020073.

[9] I. Ferrer, J. Zugazagoitia, S. Herbertz, W. John, L. Paz-Ares, G. Schmid-Bindert, KRAS-mutant non-small cell lung cancer: from biology to therapy, Lung Cancer 124 (2018) 53–64, https://doi.org/10.1016/j.lungcan.2018.07.013.

[10] X. Liu, T. Jiang, X. Li, C. Zhao, J. Li, F. Zhou, L. Zhang, S. Zhao, Y. Jia, J. Shi, G. Gao, W. Li, J. Zhao, X. Chen, C. Su, S. Ren, C. Zhou, Exosomes transmit T790M mutation-induced resistance in EGFR-mutant NSCLC by activating PI3K/AKT signalling pathway, J. Cell. Mol. Med. 24 (2020) 1529–1540, https://doi.org/10.1111/jcmm.14838.

[11] X. Zhang, M. Li, D. Lv, G. Sun, Y. Bai, H. Tian, C. Liu, Identification of a novel BRAF Thr599dup mutation in lung adenocarcinoma, Open Med (Wars). 13 (2018) 278–280, https://doi.org/10.1515/med-2018-0042.

[12] S. Pushpakom, F. Iorio, P.A. Eyers, K.J. Escott, S. Hopper, A. Wells, A. Doig, T. Guilliams, J. Latimer, C. McNamee, A. Norris, P. Sanseau, D. Cavalla, M. Pirmohamed, Drug repurposing: progress, challenges and recommendations, Nat. Rev. Drug Discov. 18 (2019) 41–58, https://doi.org/10.1038/nrd.2018.168.

[13] L. Sleire, H.E. Førde, I.A. Netland, L. Leiss, B.S. Skeie, P.Ø. Enger, Drug repurposing in cancer, Pharmacol. Res. 124 (2017) 74–91, https://doi.org/10.1016/j.phrs.2017.07.013.

[14] V. Parvathaneni, N.S. Kulkarni, A. Muth, V. Gupta, Drug Repurposing: A Promising Tool to Accelerate the Drug Discovery Process, Drug Discovery Today, 2019, https://doi.org/10.1016/j.drudis.2019.06.014.

[15] Y. Cha, T. Erez, I.J. Reynolds, D. Kumar, J. Ross, G. Koytiger, R. Kusko, B. Zeskind, S. Risso, E. Kagan, S. Papapetropoulos, I. Grossman, D. Laifenfeld, Drug repurposing from the perspective of pharmaceutical companies, Br. J. Pharmacol. 175 (2018) 168–180, https://doi.org/10.1111/bph.13798.

[16] V.R. Solomon, S. Pundir, H.-T. Le, H. Lee, Design and synthesis of novel quinacrine-[1,3]-thiazinan-4-one hybrids for their anti-breast cancer activity, Eur. J. Med. Chem. 143 (2018) 1028–1038, https://doi.org/10.1016/j.ejmech.2017.11.097.

[17] E. Kalogera, D. Roy, A. Khurana, S. Mondal, A.L. Weaver, X. He, S.C. Dowdy, V. Shridhar, Quinacrine in endometrial cancer: repurposing an old antimalarial drug, Gynecol. Oncol. 146 (2017) 187–195, https://doi.org/10.1016/j.ygyno.2017.04.022.

[18] A. Eriksson, A. Österroos, S. Hassan, J. Gullbo, L. Rickardson, M. Jarvius, P. Nygren, M. Fryknäs, M. Höglund, R. Larsson, Drug screen in patient cells suggests quinacrine to be repositioned for treatment of acute myeloid leukemia, Blood Cancer Journal. 5 (2015) e307, https://doi.org/10.1038/bcj.2015.31.

[19] A. Khurana, D. Roy, E. Kalogera, S. Mondal, X. Wen, X. He, S. Dowdy, V. Shridhar, Quinacrine promotes autophagic cell death and chemosensitivity in ovarian cancer and attenuates tumor growth, Oncotarget 6 (2015) 36354–36369, https://doi.org/10.18632/oncotarget.5632.

[20] K. Gurova, New hopes from old drugs: revisiting DNA-binding small molecules as anticancer agents, Future Oncol. 5 (2009) 1685–1704, https://doi.org/10.2217/fon.09.127.

[21] X. Wu, Y. Wang, H. Wang, Q. Wang, L. Wang, J. Miao, F. Cui, J. Wang, Quinacrine inhibits cell growth and induces apoptosis in human gastric cancer cell line SGC-7901, Curr Ther Res Clin Exp. 73 (2012) 52–64, https://doi.org/10.1016/j.curtheres.2012.02.003.

[22] J.K.T. Dermawan, K. Gurova, J. Pink, A. Dowlati, S. De, G. Narla, N. Sharma, G. R. Stark, Quinacrine overcomes resistance to erlotinib by inhibiting FACT, NF-κB, and cell-cycle progression in non-small cell lung cancer, Mol. Cancer Ther. 13 (2014) 2203–2214, https://doi.org/10.1158/1535-7163.MCT-14-0013.

[23] P. Bhateja, A. Dowlati, N. Sharma, Phase I study of the combination of quinacrine and erlotinib in patients with locally advanced or metastatic non small cell lung cancer, Investig. New Drugs 36 (2018) 435–441, https://doi.org/10.1007/s10637-017-0515-3.

[24] C.W.S. Tong, W.K.K. Wu, H.H.F. Loong, W.C.S. Cho, K.K.W. To, Drug combination approach to overcome resistance to EGFR tyrosine kinase inhibitors in lung cancer, Cancer Lett. 405 (2017) 100–110, https://doi.org/10.1016/j.canlet.2017.07.023.

[25] D.H. Truong, T.H. Tran, T. Ramasamy, J.Y. Choi, H.H. Lee, C. Moon, H.-G. Choi, C. S. Yong, J.O. Kim, Development of solid self-emulsifying formulation for improving the oral bioavailability of erlotinib, AAPS PharmSciTech 17 (2016) 466–473, https://doi.org/10.1208/s12249-015-0370-5.

[26] S.C. Baetke, T. Lammers, F. Kiessling, Applications of nanoparticles for diagnosis and therapy of cancer, Br. J. Radiol. 88 (2015) 20150207, https://doi.org/10.1259/bjr.20150207.

[27] J.K. Tee, L.X. Yip, E.S. Tan, S. Santitewagun, A. Prasath, P.C. Ke, H.K. Ho, D. T. Leong, Nanoparticles' interactions with vasculature in diseases, Chem. Soc. Rev. 48 (2019) 5381–5407, https://doi.org/10.1039/c9cs00309f.

[28] F. Danhier, E. Ansorena, J.M. Silva, R. Coco, A. Le Breton, V. Préat, PLGA-based nanoparticles: an overview of biomedical applications, J. Control. Release 161 (2012) 505–522, https://doi.org/10.1016/j.jconrel.2012.01.043.

[29] N.-E. Ryu, S.-H. Lee, H. Park, Spheroid culture system methods and applications for mesenchymal stem cells, Cells. 8 (2019) 1620, https://doi.org/10.3390/cells8121620.

[30] Y. Yang, Y. Cheng, S. Peng, L. Xu, C. He, F. Qi, M. Zhao, C. Shuai, Microstructure evolution and texture tailoring of reduced graphene oxide reinforced Zn scaffold, Bioactive Materials. 6 (2021) 1230–1241, https://doi.org/10.1016/j.bioactmat.2020.10.017.

[31] B. Vaidya, V. Parvathaneni, N.S. Kulkarni, S.K. Shukla, J.K. Damon, A. Sarode, D. Kanabar, J.V. Garcia, S. Mitragotri, A. Muth, V. Gupta, Cyclodextrin modified erlotinib loaded PLGA nanoparticles for improved therapeutic efficacy against non-small cell lung cancer, Int. J. Biol. Macromol. 122 (2019) 338–347, https://doi.org/10.1016/j.ijbiomac.2018.10.181.

[32] B. Vaidya, N.S. Kulkarni, S.K. Shukla, V. Parvathaneni, G. Chauhan, J.K. Damon, A. Sarode, J.V. Garcia, N. Kunda, S. Mitragotri, V. Gupta, Development of inhalable quinacrine loaded bovine serum albumin modified cationic nanoparticles: repurposing quinacrine for lung cancer therapeutics, Int. J. Pharm. 577 (2020) 118995, https://doi.org/10.1016/j.ijpharm.2019.118995.

[33] S.K. Shukla, N.S. Kulkarni, A. Chan, V. Parvathaneni, P. Farrales, A. Muth, V. Gupta, Metformin-encapsulated liposome delivery system: an effective treatment approach against breast cancer, Pharmaceutics. 11 (2019) 559, https://doi.org/10.3390/pharmaceutics11110559.

[34] N.S. Kulkarni, V. Parvathaneni, S.K. Shukla, L. Barasa, J.C. Perron, S. Yoganathan, A. Muth, V. Gupta, Tyrosine Kinase Inhibitor Conjugated Quantum Dots for Non-small Cell Lung Cancer (NSCLC) Treatment, European Journal of Pharmaceutical Sciences, 2019, https://doi.org/10.1016/j.ejps.2019.03.026.

[35] V. Parvathaneni, N.S. Kulkarni, S.K. Shukla, P.T. Farrales, N.K. Kunda, A. Muth, V. Gupta, Systematic development and optimization of inhalable pirfenidone liposomes for non-small cell lung cancer treatment, Pharmaceutics. 12 (2020) 206, https://doi.org/10.3390/pharmaceutics12030206.
[36] N.S. Kulkarni, B. Vaidya, V. Parvathaneni, D. Bhanja, V. Gupta, Repurposing quinacrine for treatment of malignant mesothelioma: in-vitro therapeutic and mechanistic evaluation, Int. J. Mol. Sci. 21 (2020) 6306, https://doi.org/10.3390/ijms21176306.
[37] Q. Geissmann, OpenCFU, a new free and open-source software to count cell colonies and other circular objects, PLoS One 8 (2013), e54072, https://doi.org/10.1371/journal.pone.0054072.
[38] S.K. Shukla, N.S. Kulkarni, P. Farrales, D.D. Kanabar, V. Parvathaneni, N.K. Kunda, A. Muth, V. Gupta, Sorafenib loaded inhalable polymeric nanocarriers against non-small cell lung cancer, Pharmaceutical Research 37 (2020), https://doi.org/10.1007/s11095-020-02790-3.
[39] V. Parvathaneni, M. Goyal, N.S. Kulkarni, S.K. Shukla, V. Gupta, Nanotechnology based repositioning of an anti-viral drug for non-small cell lung cancer (NSCLC), Pharmaceutical Research 37 (2020), https://doi.org/10.1007/s11095-020-02848-2.
[40] H. Kang, S. Rho, W.R. Stiles, S. Hu, Y. Baek, D.W. Hwang, S. Kashiwagi, M.S. Kim, H.S. Choi, Size-dependent EPR effect of polymeric nanoparticles on tumor targeting, Adv Healthc Mater. 9 (2020), e1901223, https://doi.org/10.1002/adhm.201901223.
[41] W. Wang, J.-N. Gallant, S.I. Katz, N.G. Dolloff, C.D. Smith, J. Abdulghani, J. E. Allen, D.T. Dicker, B. Hong, A. Navaraj, W.S. El-Deiry, Quinacrine sensitizes hepatocellular carcinoma cells to TRAIL and chemotherapeutic agents, Cancer Biol. Ther. 12 (2011) 229–238, https://doi.org/10.4161/cbt.12.3.17033.
[42] T.-C. Chou, Drug combination studies and their synergy quantification using the Chou-Talalay method, Cancer Res. 70 (2010) 440–446, https://doi.org/10.1158/0008-5472.CAN-09-1947.
[43] J.Y. Kim, H.S. Kim, S. Yoon, Tyrosine kinase inhibitors imatinib and erlotinib increase apoptosis of antimitotic drug-resistant KBV20C cells without inhibiting P-gp, Anticancer Res. 39 (2019) 3785–3793, https://doi.org/10.21873/anticanres.13527.
[44] S. Barth, D. Glick, K.F. Macleod, Autophagy: assays and artifacts, J. Pathol. 221 (2010) 117–124, https://doi.org/10.1002/path.2694.
[45] N. Karachaliou, J. Codony-Servat, J.W.P. Bracht, M. Ito, M. Filipska, C. Pedraz, I. Chaib, J. Bertran-Alamillo, A.F. Cardona, M.A. Molina, R. Rosell, Characterising acquired resistance to erlotinib in non-small cell lung cancer patients, Expert Rev Respir Med. 13 (2019) 1019–1028, https://doi.org/10.1080/17476348.2019.1656068.
[46] A.F. Cardona, O. Arrieta, M.I. Zapata, L. Rojas, B. Wills, N. Reguart, N. Karachaliou, H. Carranza, C. Vargas, J. Otero, P. Archila, C. Martín, L. Corrales, M. Cuello, C. Ortiz, L.E. Pino, R. Rosell, Z.L. Zatarain-Barrón, CLICaP, acquired resistance to erlotinib in EGFR mutation-positive lung adenocarcinoma among Hispanics (CLICaP), Target. Oncol. 12 (2017) 513–523, https://doi.org/10.1007/s11523-017-0497-2.
[47] C. Ma, S. Wei, Y. Song, T790M and acquired resistance of EGFR TKI: a literature review of clinical reports, J Thorac Dis. 3 (2011) 10–18, https://doi.org/10.3978/j.issn.2072-1439.2010.12.02.
[48] C. Masuda, M. Yanagisawa, K. Yorozu, M. Kurasawa, K. Furugaki, N. Ishikura, T. Iwai, M. Sugimoto, K. Yamamoto, Bevacizumab counteracts VEGF-dependent resistance to erlotinib in an EGFR-mutated NSCLC xenograft model, Int. J. Oncol. 51 (2017) 425–434, https://doi.org/10.3892/ijo.2017.4036.
[49] R. Preet, P. Mohapatra, S. Mohanty, S.K. Sahu, T. Choudhuri, M.D. Wyatt, C. N. Kundu, Quinacrine has anticancer activity in breast cancer cells through inhibition of topoisomerase activity, Int. J. Cancer 130 (2012) 1660–1670, https://doi.org/10.1002/ijc.26158.
[50] P. Mohapatra, R. Preet, D. Das, S.R. Satapathy, T. Choudhuri, M.D. Wyatt, C. N. Kundu, Quinacrine-mediated autophagy and apoptosis in colon cancer cells is through a p53- and p21-dependent mechanism, Oncol. Res. 20 (2012) 81–91.
[51] Y. Wang, Q. Bi, L. Dong, X. Li, X. Ge, X. Zhang, J. Fu, D. Wu, S. Li, Quinacrine enhances cisplatin-induced cytotoxicity in four cancer cell lines, Chemotherapy. 56 (2010) 127–134, https://doi.org/10.1159/000313525.
[52] J.-N. Gallant, J.E. Allen, C.D. Smith, D.T. Dicker, W. Wang, N.G. Dolloff, A. Navaraj, W.S. El-Deiry, Quinacrine synergizes with 5-fluorouracil and other therapies in colorectal cancer, Cancer Biol. Ther. 12 (2011) 239–251, https://doi.org/10.4161/cbt.12.3.17034.
[53] J. Xue, Z. Guan, X. Zhu, J. Lin, C. Cai, X. Jin, Y. Li, Z. Ye, W. Zhang, X. Jiang, Cellular internalization of polypeptide-based nanoparticles: effects of size, shape and surface morphology, Biomater Sci. 6 (2018) 3251–3261, https://doi.org/10.1039/c8bm01163j.
[54] H.K. Makadia, S.J. Siegel, Poly lactic-co-glycolic acid (PLGA) as biodegradable controlled drug delivery carrier, Polymers. 3 (2011) 1377–1397, https://doi.org/10.3390/polym3031377.
[55] J. Ahlawat, G. Henriquez, M. Narayan, Enhancing the delivery of chemotherapeutics: role of biodegradable polymeric nanoparticles, Molecules 23 (2018), https://doi.org/10.3390/molecules23092157.
[56] A.A. Ranade, P.P. Bapsy, S. Nag, D. Raghunadharao, V. Raina, S.H. Advani, S. Patil, A. Maru, V.P. Gangadharan, C. Goswami, J.S. Sekhon, K. Sambasivaiah, P. Parikh, A. Bakshi, R. Mohapatra, A multicenter phase II randomized study of Cremophor-free polymeric nanoparticle formulation of paclitaxel in women with locally advanced and/or metastatic breast cancer after failure of anthracycline: nanoparticle paclitaxel efficacy study, Asia-Pacific Journal of Clinical Oncology 9 (2013) 176–181, https://doi.org/10.1111/ajco.12035.
[57] J. Kondo, T. Ekawa, H. Endo, K. Yamazaki, N. Tanaka, Y. Kukita, H. Okuyama, J. Okami, F. Imamura, M. Ohue, K. Kato, T. Nomura, A. Kohara, S. Mori, S. Dan, M. Inoue, High-throughput screening in colorectal cancer tissue-originated spheroids, Cancer Sci. 110 (2019) 345–355, https://doi.org/10.1111/cas.13843.
[58] C.-H. Wassmer, K. Bellofatto, L. Perez, V. Lavallard, D. Cottet-Dumoulin, S. Ljubicic, G. Parnaud, D. Bosco, E. Berishvili, F. Lebreton, Engineering of primary pancreatic islet cell spheroids for three-dimensional culture or transplantation: a methodological comparative study, Cell Transplant. 29 (2020), 096368972093729, https://doi.org/10.1177/0963689720937292.